Acta Oceanol. Sin., 2018, Vol. 37, No. 6, P. 1–10
DOI: 10.1007/s13131-018-1217-1
http://www.hyxb.org.cn
E-mail: hyxbe@263.net

Validation of significant wave height retrieval from co-polarization Chinese Gaofen-3 SAR imagery using an improved algorithm

SHENG Yexin[1], SHAO Weizeng[1]*, ZHU Shuai[1], SUN Jian[2], YUAN Xinzhe[3], LI Shuiqing[4, 5], SHI Jian[6], ZUO Juncheng[1]

[1] Marine Science and Technology College, Zhejiang Ocean University, Zhoushan 316000, China

[2] Physical Oceanography Laboratory/CIMST, Ocean University of China and Qingdao National Laboratory for Marine Science and Technology, Qingdao 266100, China

[3] National Satellite Ocean Application Service, State Oceanic Administration, Beijing 100081, China

[4] Institute of Oceanology, Chinese Academy of Sciences, Qingdao 266071, China

[5] Laboratory for Ocean Dynamics and Climate, Qingdao National Laboratory for Marine Science and Technology, Qingdao 266071, China

[6] College of Meteorology and Oceanography, National University of Defense Technology, Nanjing 210007, China

Received 23 January 2018; accepted 21 March 2018

Abstract

Chinese Gaofen-3 (GF-3) is the first civilian satellite to carry C-band (5.3 GHz) synthetic aperture radar (SAR). During the period of August 2016 to December 2017, 1 523 GF-3 SAR images acquired in quad-polarization (vertical-vertical (VV), horizontal-horizontal (HH), vertical-horizontal (VH), and horizontal-vertical (HV)) mode were recorded, mostly around China's seas. In our previous study, the root mean square error (RMSE) of significant wave height (SWH) was found to be around 0.58 m when compared with retrieval results from a few GF-3 SAR images in co-polarization (VV and HH) with moored measurements by using an empirical algorithm CSAR_WAVE. We collected a number of sub-scenes from these 1 523 images in the co-polarization channel, which were collocated with wind and SWH data from the European Centre for Medium-Range Weather Forecasts (ECMWF) reanalysis field at a 0.125° grid. Through the collected dataset, an improved empirical wave retrieval algorithm for GF-3 SAR in co-polarization was tuned, herein denoted as CSAR_WAVE2. An additional 92 GF-3 SAR images were implemented in order to validate CSAR_WAVE2 against SWH from altimeter Jason-2, showing an about 0.52 m RMSE of SWH for co-polarization GF-3 SAR. Therefore, we conclude that the proposed empirical algorithm has a good performance for wave retrieval from GF-3 SAR images in co-polarization.

Key words: Gaofen-3, synthetic aperture radar, significant wave height

Citation: Sheng Yexin, Shao Weizeng, Zhu Shuai, Sun Jian, Yuan Xinzhe, Li Shuiqing, Shi Jian, Zuo Juncheng. 2018. Validation of significant wave height retrieval from co-polarization Chinese Gaofen-3 SAR imagery using an improved algorithm. Acta Oceanologica Sinica, 37(6): 1–10, doi: 10.1007/s13131-018-1217-1

1 Introduction

It is well known that synthetic aperture radar (SAR) has the capability of wind and wave monitoring (Chapron et al., 2001) in large swath coverage with a fine spatial resolution, especially in extreme sea states (Li et al., 2002; Hwang and Fois, 2015; Li, 2015; Shao et al., 2017a). To date, SAR data is available at C-band (5.3 GHz) Canadian Radarsat-2 (R-2), and European Sentinel-1 (S-1); X-band (9.8 GHz) German TerraSAR-X/TanDEM-X, Italian Cosmo-SkyMed and Korean Kompsat-5; and L-band (1.2 GHz) Japanese ALOS-2 satellite. Gaofen-3 (GF-3) SAR at C-band was launched by the China Academy of Space Technology (CAST) in August 2016, and can operate in 12 imaging modes with a fine spatial resolution of image up to 1 m. It has a 755-km orbit height above the earth's surface with a 26-day repeat cycle. Recently, preliminary analysis of marine applications using GF-3 SAR data have been achieved, in particular, for wind (Wang et al., 2017; Ren et al., 2017; Shao et al., 2018) and wave monitoring (Yang et al., 2017; Shao et al., 2017b).

Based on a good understanding of the wave imaging mechanism on SAR, including tilt modulation (Lyzenga, 1986), hydrodynamic modulation (Feindt et al., 1986) and velocity bunching (Alpers et al., 1981; Alpers and Bruening, 1986), wave retrieval algorithms have been thoroughly studied over recent decades. Basic scattering physics is widely used in theoretical-based wave retrieval algorithms, e.g., Max-Planck Institute Algorithm (MPI) (Hasselmann and Hasselmann, 1991; Hasselmann et al., 1996), the semi parametric retrieval algorithm (SPRA) (Mastenbroek and De Valk, 2000), the parameterized first-guess spectrum method (PFSM) (Sun and Guan, 2006; Shao et al., 2015; Lin et al., 2017) and the partition rescaling and shift algorithm (PARSA)

Foundation item: The National Key Research and Development Program of China under contract Nos 2016YFC1401905 and 2017YFA0604901; the National Natural Science Foundation of China under contract Nos 41776183, 41676014, 41606024 and 41506033; the National Social Science Foundation of China under contract No. 15ZDB170.
*Corresponding author, E-mail: shaoweizeng@zjou.edu.cn

(Schulz-Stellenfleth et al., 2005; Li et al., 2010), which are independent of radar frequency and imaging polarization. However, velocity bunching is a non-linear modulation, that causes waves of a shorter than specific wavelength to be undetectable in the azimuth direction (or satellite flight direction) and a cutoff in the SAR intensity spectrum (Alpers and Bruening, 1986; Hasselmann and Hasselmann, 1991). The idea behind these theoretical-based algorithms is directly inverting the SAR intensity spectrum into the wave spectrum after employing a "first-guess" wave spectrum, which is considered to be the compensation for loss in the SAR intensity spectrum due to non-linear effect of velocity bunching. The algorithms MPI and PARSA take the simulation from a numeric wave model, while a prior wave spectrum is produced by using a parameterized empirical function in the schemes of algorithms SPRA and PFSM, such as the Jonswap spectrum (Hasselmann and Hasselmann, 1985). Therefore, they are limitedly applied in the operation system, because the quality of the "first-guess" wave spectrum determines the SAR-derived wave spectrum. Moreover the "first-guess" wave spectrum is not reliable in the presence of other marine phenomena. Ocean wave parameters, e.g., significant wave height (SWH) and mean wave period (MWP), are calculated from the SAR-derived wave spectrum.

An empirical wave retrieval algorithm for C-band ERS SAR is proposed by Schulz-Stellenfleth et al. (2007), denoted as CWAVE_ERS. In particular, CWAVE has been tuned for ENVISAT Advanced SAR (ASAR) (Li et al., 2011) and S-1 SAR (Stopa and Mouche, 2017). The CWAVE model is designed to be an empirical function, in which the sea state parameter SWH is connected with a set of variables, including normalized radar cross section (NRCS), variance of the normalized SAR image and several orthonormal functions derived from the two-dimensional SAR spectrum. The advantage is that SWH can be directly retrieved from SAR without calculating the modulation transfer function (MTF) of each SAR mapping modulation. However, CWAVEs have only been validated for SAR data acquired in wave mode until now. Following the idea of CWAVE, researchers have recently exploited the empirical algorithms XWAVE for X-band SAR (Bruck and Lehner, 2015; Pleskachevsky et al., 2016; Shao et al., 2017c).

Recent research has revealed that the azimuthal cutoff wavelength is derived to be proportional to the second moment of a wave spectrum (Hasselmann and Hasselmann, 1991; Marghany et al., 2002). On the other hand, SWH is calculated by integrating a wave spectrum according to traditional wave theory. Therefore, SWH is theoretically related to cutoff wavelength in the azimuth direction. Interestingly, several studies have made an attempt to retrieve SWH through azimuthal cutoff wavelength (Wang et al., 2012; Ren et al., 2015; Grieco et al., 2016; Stopa et al., 2016). The dependences of radar incidence angle and wave propagation direction on azimuthal cutoff wavelength were investigated in our previous study using theoretical analysis and simulation experiment (Shao et al., 2016). Then we constructed an empirical wave retrieval algorithm, denoted as CSAR_WAVE, which was tuned through VV-polarization S-1 SAR image and collocated measurements from the National Data Buoy Center (NDBC) buoys of the National Oceanic and Atmospheric Administration (NOAA). The preliminary assessment showed that CSAR_WAVE is applicable for GF-3 SAR with around 0.58 m root mean square error (RMSE) of the retrieved SWH compared with the NDBC buoy measurements of NOAA (Shao et al., 2017b). However, the accuracy of the retrieval results is expected to be further improved for the operational application of GF-3 SAR, as the SAR-derived product is dedicated to oceanography research, especially in coastal waters. Therefore, in this study, we have developed an improved wave retrieval algorithm for GF-3 SAR in co-polarization (VV and HH).

The remaining part of this paper is organized as follows: collected datasets are briefly described in Section 2. Section 3 shows the methodology of derivation of the empirical algorithm. In this section, the process of tuning the empirical algorithm for co-polarization GF-3 SAR is also presented. Then the validation of the retrieved SWHs using the proposed algorithm and other three existing empirical algorithms, are shown in Section 4. Conclusions are summarized in Section 5.

2 Description of dataset

Since GF-3 SAR was launched in 2016 by CAST, during the period of August 2016 to December 2017 a number of images acquired in quad-polarization mode (QPS-I/II) (vertical-vertical (VV), horizontal-horizontal (HH), vertical-horizontal (VH), and horizontal-vertical (HV)) have been recorded. Most of these GF-3 SAR images were located around China's seas and they were processed as Level-1A (L-1A) products, which have a standard pixel of 8 m and 25 m for QPS-I and QPS-II mode, respectively. Because the SAR backscattering signature from a sea surface in co-polarization is more sensitive than that in cross-polarization (VH and HV), the collected GF-3 SAR images in VV- and HH-polarization channel are used in our study. Equation 1 is used for calculating the NRCS of a co-polarization GF-3 SAR intensity image.

$$\sigma^0 = DN^2 \left(\frac{M}{32\,767}\right)^2 - N, \tag{1}$$

where σ^0 is the NRCS united in dB, DN is the SAR-measured intensity, M and N are the calibrated constants stored in the annotated file with the original SAR intensity image.

As an example, a quick-look image of the calibrated GF-3 SAR image acquired in QPS-I mode at 10:40 UTC on 18 January 2017 in VV- and HH-polarization is shown in Fig. 1a and Fig. 1b, respectively. It was found that wind direction is vertical to two-dimensional SAR image spectra for wavelengths between 800 m and 3 000 m at peaks (Alpers and Brümmer, 1994), indicating wind direction can be directly measured from SAR. However, the SAR-derived wind direction has a 180° ambiguity. The European Centre for Medium-Range Weather Forecasts (ECMWF) provides global reanalysis wind data with a fine spatial resolution of 0.125°×0.125° at intervals of six hours, which is employed to remove that ambiguity. The wind speed (U_{10}) at 10 m-height above sea surface can be inverted by using the combination method proposed in our previous study (Shao et al., 2014), which is based on the geophysical model function (GMF) CMOD5 (Hersbach et al., 2007) and CMOD4 (Stoffelen and Anderson, 1997). The colored vectors shown in Fig. 1 represent the SAR-derived wind fields. Note that it is necessary to use the polarization ratio (PR) at C-band (Zhang et al., 2011) together with GMF to retrieve the wind field from an HH-polarization GF-3 SAR image.

In our study, all the GF-3 SAR images are divided into a number of sub-scenes with a spatial coverage of about 5 km×5 km. These extracted sub-scenes are collocated with 0.125° gridded ECMWF reanalysis wave data at intervals of six hours. It is necessary to ensure that the sub-scenes covering the locations of the ECMWF reanalysis grids data are calculated by bilinear interpolation in temporal scale, as there is a time difference between the GF-3 SAR imaging time and the interval time of the ECMWF

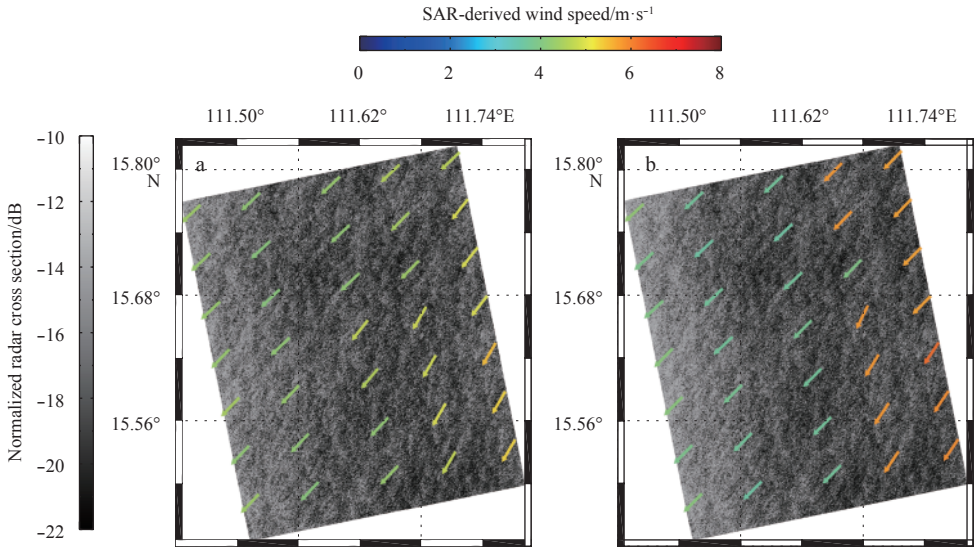

Fig. 1. The quick-look image of calibrated GF-3 SAR image at 10:40 UTC on 18 January 2017, in which colored vectors represent the SAR-derived wind fields. a. VV-polarization and b. HH-polarization.

reanalysis grids data. Then we have more than ten thousand matchups, which are treated as a dataset for tuning an improved algorithm for wave retrieval from GF-3 SAR images. Figure 2 shows the ECMWF reanalysis wind and wave map at 06:00 UTC on 18 January 2017, in which the black rectangle represents the spatial coverage of a GF-3 SAR image located in the South China Sea as exhibited in Fig.1. It should be noted that the SWH from the ECMWF reanalysis data goes up to 4 m, therefore, GF-3 SAR images at low to moderate sea states are included in the dataset. Recently, a new approach for SWH retrieval in hurricanes has been constructed through studying the relationship between SWH and NRCS (Romeiser et al., 2015). As mentioned by the authors, this is still to be improved due to the complicated non-linear effect of waves at extreme sea states.

The high-precision ocean altimetry on Jason-2 launched in 2008 is a marine observation system over global sea, which is a follow-on satellite of the oceanography monitoring mission of Jason-1. So far, Operational Geophysical Data Record (OGDR) derived from the Jason-2 satellite track is a near real-time operational product, in particular including more reliable SWH data which is better than that of Jason-1 by about 7% (Abdalla et al., 2010). This high-quality product is essentially dedicated to oceanography research. An additional 91 quad-polarization GF-3 SAR images were collected and these GF-3 SAR images cover the footprints of altimeter Jason-2, which were implemented in order to validate the improved algorithm in our study.

3 Methodology

In this section, the methodology of derivation of an improved algorithm is presented, which is based on two existing empirical wave retrieval algorithms CWAVE and CSAR_WAVE. Then the improved algorithm, denoted CSAR_WAVE2, is tuned for co-po-

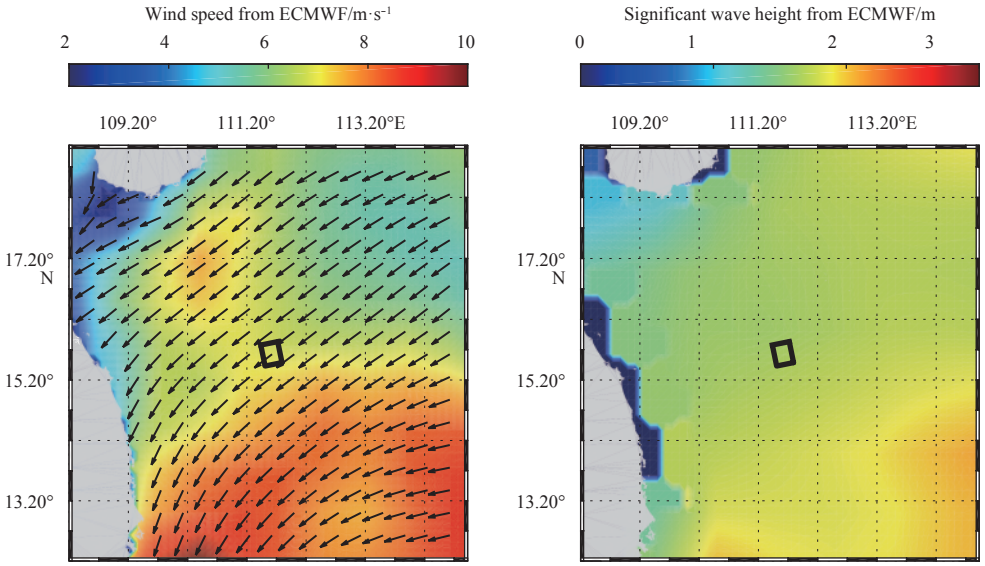

Fig. 2. The 0.125° gridded ECMWF reanalysis data at 06:00 UTC on 18 January 2017, in which rectangles represent the spatial coverage of a GF-3 SAR image located in the South China Sea. a. ECMWF wind map and b. ECMWF wave map.

larization GF-3 SAR.

3.1 *Algorithm CWAVE*

As mentioned in Section 1, algorithms MPI, SPRA, PFSM and PARSA rely on prior information on a wave spectrum, e.g., numeric simulation from a wave model and computation from a parametric wave function. In the operational application, they take some time to produce a "first-guess" wave spectrum and on the non-linear inversion of an SAR spectrum into a wave spectrum (Hasselmann and Hasselmann, 1991; Hasselmann et al., 1996). Moreover, it is difficult to improve the accuracy of SWH retrieval in the physics aspect of theoretical-based algorithms. In practice, empirical models are routine operations for marine applications of Scatterometer and SAR, such as GMFs for wind retrieval (Stoffelen and Anderson, 1997; Hersbach et al., 2007). The GMF CWAVE family, e.g., CWAVE_ERS (Schulz-Stellenfleth et al., 2007) for ERS SAR and CWAVE_ENV (Li et al., 2011) for ENVISAT-ASAR, were originally exploited by the SAR oceanography group at the German Aerospace Center (DLR), which allows for direct retrieval of wave parameters from SAR wave mode data without calculating the complex MTF of each SAR mapping modulation.

In a SAR image, sea state measurement S can be determined by a set of imaging parameters s_i (s_1, s_2, ..., s_n) with a coefficient vector a_i (a_0, a_1, ..., a_n). Due to the modulation of velocity bunching, non-linearity among different imaging parameters is also included by adding the products of different imaging parameters s_i with a coefficient vector $a_{i,j}$ ($i \leqslant j \leqslant n$). Based on this assumption, the function of CWAVE principally follows the multiple-regression method stated as

$$S = a_0 + \sum_{i=1}^{n} a_i \times s_i + \sum_{i,j=1}^{n} a_{i,j} \times s_i \times s_j. \tag{2}$$

In the CWAVE models, imaging parameters s_i include NRCS σ_0, and variance of the normalized SAR image *cvar*, both of which directly contribute to sea state, and a set of orthonormal functions derived from the two-dimensional SAR spectrum. *cvar* is defined as follows:

$$cvar = \mathrm{var}\left(\frac{I - \bar{I}}{\bar{I}}\right), \tag{3}$$

where I is the pixel intensity of a SAR image and $\bar{I}$ is the average of I. The coefficients in CWAVE models were tuned for ERS and ENVISAT-ASAR wave mode data acquired in VV-polarization at a fixed incidence angle of 23°. Therefore, CWAVE needs to be retuned for other SAR data at various incidence angles, such as CWAVE_S1 for S-1 SAR (Stopa and Mouche, 2017).

3.2 *Algorithm CSAR_WAVE*

The relationship between cutoff wavelength in azimuth direction λ_c and SWH was demonstrated in the study proposed by Hasselmann and Hasselmann (1991):

$$\lambda_c = \pi\beta\sqrt{\int |T_\omega^v|^2 S_\omega \mathrm{d}\omega}, \tag{4}$$

where β is the satellite range-to-velocity parameter, $|T_\omega^v|$ is the velocity bunching transfer function, ω is wave frequency and S_ω is the one-dimensional wave spectrum. In the imaging process, λ_c can be estimated by fitting a one-dimensional SAR spectrum with a Gaussian fit function (Sun and Kawamura, 2009). The Gaussian fit function has the formulation $\exp\{\pi(k_x/k_c)\}$, in which k_x is the azimuthal wavenumber and $k_c = 2\pi/\lambda_c$ is the azimuthal cutoff wavenumber. Through analyzing a number of recorded ENVISAT-ASAR wave mode data, recent research has revealed that λ_c provides meaningful information about the sea state, even at large sea states (>250 m) (Stopa et al., 2016).

SWH can be calculated by integrating wave spectrum S_ω,

$$SWH = 4\sqrt{\int S_\omega \mathrm{d}\omega}. \tag{5}$$

Theoretically, SWH is related to λ_c through the above two equations. Recently, several algorithms have been developed by using the λ_c to estimate SWH for ENVISAT-ASAR (Wang et al., 2012), quad-polarization R-2 SAR (Ren et al., 2015) and S-1 SAR (Grieco et al., 2016; Stopa and Mouche, 2017).

The dependency of λ_c, radar incidence angle θ and peak wave direction relative to range direction φ on SWH was simulated through the widely used Jonswap wave spectrum model (Hasselmann and Hasselmann, 1985). It was found that SWH is linearly related with λ_c/β, while SWH has a positive and negative relationship with θ and φ respectively (Shao et al., 2016). The semi-empirical wave retrieval algorithm, denoted as CSAR_WAVE, was originally developed for S-1 SAR in our previous study. The formulation of CSAR_WAVE is designed as a first-order linear function,

$$SWH = \left(\frac{\lambda_c}{\beta}\right)(A_1 + A_2 \sin\theta + A_3 \cos 2\varphi) + A_4, \tag{6}$$

where coefficients A are determined from S-1 SAR image collocated NDBC buoys of NOAA. It was reported by Shao et al. (2017b) that the RSME of SWH is 0.58 m and 0.57 m when using CSAR_WAVE for GF-3 SAR in VV- and HH-polarization respectively, as the retrieved SWHs are validated against the NDBC buoys of NOAA around U.S. waters.

3.3 *Tuning the improved algorithm*

In order to enhance the sensitivity of non-linearity on SWH in an empirical algorithm, the formulation of a CWAVE model is basically employed. However, imaging parameters s_i in the CWAVE model are set as a vector (U_{10}, σ_0, *cvar*, λ_c/β, $\sin\theta$, $\cos 2\varphi$, λ_{SAR}) for practical application, in which three factors, e.g., U_{10}, σ_0 (united in dB) and *cvar*, are directly related with sea state (Li et al., 2010; Grieco et al., 2016; Stopa et al., 2016). Besides, the dependences of other factors on SWH, including λ_c/β, θ and φ, have been already investigated by Shao et al. (2016). In particular, λ_{SAR} represents the SAR length at peaks of the SAR spectrum, which is also assumed to be an essential factor in SWH, according to the derivation model through the SAR imaging mechanism of ocean wave, as referred to in Eq. (16) proposed by Wang et al. (2012).

In total, we have obtained more than ten thousand subscenes extracted from GF-3 images in co-polarization channel with collocated ECMWF reanalysis SWH data. During the process, three variables, i.e., λ_c, φ and λ_{SAR}, were derived from the SAR intensity spectrum. The sub-scene extracted from the case exhibited in Fig. 1, which is acquired in VV-polarization, is shown in Fig. 3a. The corresponding two-dimensional SAR spectrum of the sub-scene is shown in Fig. 3b, in which φ and λ_{SAR} can be dir-

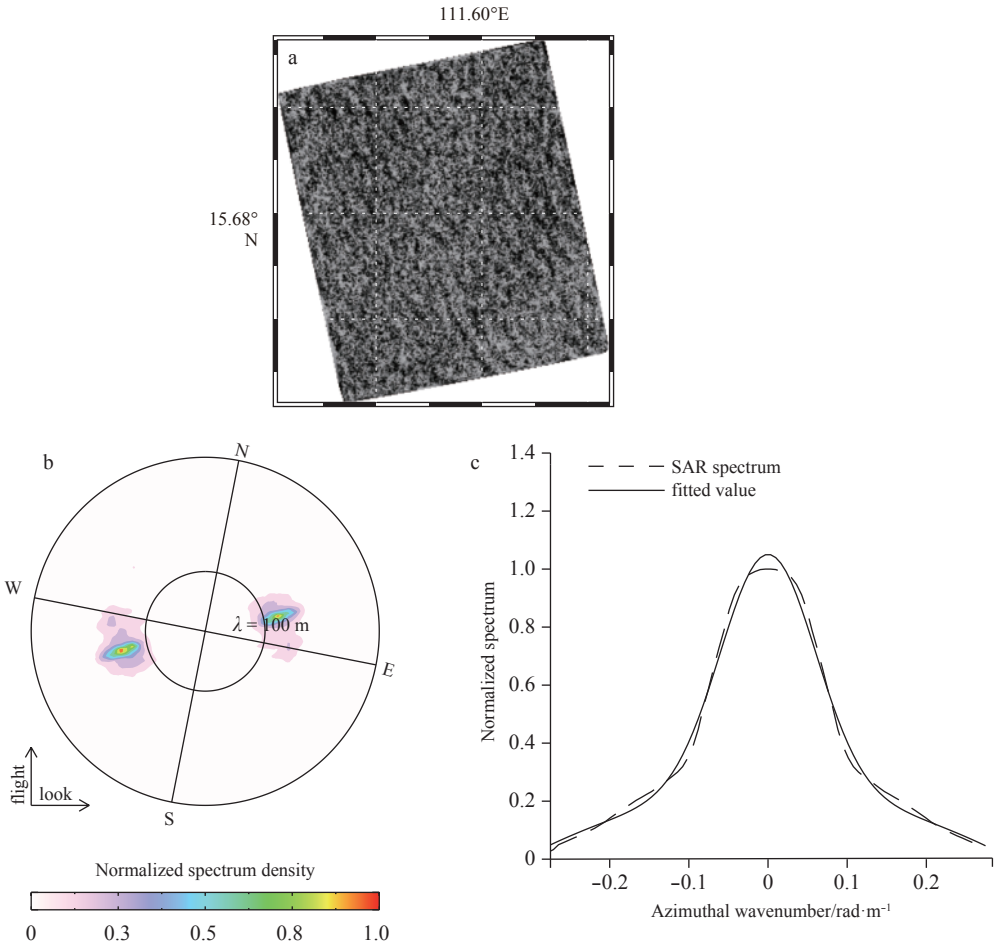

Fig. 3. The sub-scene extracted from the case in VV-polarization, which was taken on 18 January 2017 at 10:40 UTC (a); the two-dimensional SAR spectra of sub-scene in polar coordinate (b); and the Gaussian fitted result of sub-scene (c).

ectly obtained. The Gaussian fitted result of λ_c is illustrated in Fig. 3c.

The matchup dataset is used to determine the 36 coefficients $a_{i,j}$ ($i \leqslant j \leqslant 7$) in Eq. (2) by using the least-squares method, in which subscripts (1, 2, ..., 7) represent the corresponding variables (U_{10}, σ_0, *cvar*, λ_c/β, $\sin\theta$, $\cos 2\varphi$, λ_{SAR}), e.g., a_{12} is the coefficient for the term of $U_{10}\times\sigma_0$. The tuned results in the improved algorithm, denoted as CSAR_WAVE2, are shown in Table 1 for co-polarization GF-3 SAR.

Figure 4 shows the fitting results of CSAR_WAVE2 compared with ECMWF reanalysis SWH in our data collection. It is found that the correlation (COR) between the ECMWF reanalysis data and the simulated values is around 0.72 for co-polarization GF-3 SAR. Under these circumstances, we think the improved algorithm CSAR_WAVE2 is suitable for SWH retrieval from co-polarization GF-3 SAR images.

4 Validation

With reference to the application process of existing CWAVE and CSAR_WAVE models, the process of SWH retrieval by our use of CSAR_WAVE2 is roughly illustrated in Fig. 5. We first show the quick-look image of the VV-polarization GF-3 SAR image acquired at 20:49 UTC on 26 July 2017 in Fig. 6a. The inverted wave map for this case when using CSAR_WAVE2 is shown in Fig. 6b, in which the several small colored rectangles represent the SWH data measured from the altimeter Jason-2 footprints. It is found that the SAR-derived SWH is close to the SWH data of Jason-2. In particular, the trend of the inverted wave map is consistent with that following the track of the Jason-2 footprints.

In addition, we have applied CSAR_WAVE2 to a total of 91 available GF-3 SAR images and compared the results with those from the SWH data from altimeter Jason-2. In Fig. 7, the RMSE of SWH is 0.51 m for VV-polarization and the RMSE of SWH is 0.52 m for HH-polarization. The reported accuracy of SWH for C-band SAR is an RMSE of SWH of 0.55 m as validated against measurements from moored buoys using the PFSM algorithm (Lin et al., 2017) and RMSE is 0.51 m when comparing the wave retrievals with the WAM model predictions (Schulz-Stellenfleth et al., 2005) using the PARSA algorithm. It is indicated that CSAR_WAVE2 has a better accuracy of SWH retrieval than that using theoretical-based algorithms. In particular, it is applicable without calculating the complex MTF of each mapping modulation.

We also compared the SAR-derived results with SWH from Jason-2 by using the existing three empirical algorithms proposed by Wang et al. (2012), Ren et al. (2015) and Grieco et al. (2016). All of these algorithms were developed based on azimuthal cutoff wavelength and tuned through R-2 and S-1 SAR data acquired in VV-polarization. Figure 8 shows that the RMSE of SWH is 0.70 m, 0.62 m and 0.61 m using the algorithms by Wang et al. (2012), Ren et al. (2015) and Grieco et al. (2016), respectively. And a comparison between SAR-derived SWHs and measure-

Table 1. The coefficients of CSAR_WAVE2 for GF-3 SAR

Coefficient	VV-polarization, HH-polarization	Coefficient	VV-polarization, HH-polarization	Coefficient	VV-polarization, HH-polarization
a_0	4.550 081, 4.685 711	a_{15}	0.395 260, 0.661 365	a_{36}	–0.000 948, –0.023 572
a_1	–0.117 950, –0.037 123	a_{16}	0.021 143, 0.013 080	a_{37}	0.000 017, –0.000 881
a_2	–0.037 560, –0.123 305	a_{17}	–0.000 051, –0.000 101	a_{44}	–0.215 274, 0.018 952
a_3	0.003 769, –2.008 078	a_{22}	0.002 117, 0.000 932	a_{45}	–2.068 321, 1.062 604
a_4	1.422 161, 1.487 999	a_{23}	–0.000 256, –0.057 926	a_{46}	0.270 182, 0.290 735
a_5	–14.158 478, –17.544 858	a_{24}	–0.015 345, 0.088 712	a_{47}	0.000 401, 0.000 192
a_6	0.046 233, –0.243 763	a_{25}	0.156 521, 0.068 177	a_{55}	11.135 928, 9.447 940
a_7	–0.006 104, –0.007 993	a_{26}	0.025 062, 0.013 996	a_{56}	0.743 692, 0.926 733
a_{11}	–0.003 169, –0.006 690	a_{27}	0.000 145, 0.000 049	a_{57}	0.017 372, 0.017 870
a_{12}	0.000 329, 0.009 146	a_{33}	0.000 004, –0.000 050	a_{66}	0.080 189, 0.042 562
a_{13}	0.000 089, 0.037 343	a_{34}	–0.000 495, 0.174 004	a_{67}	–0.002 490, –0.002 032
a_{14}	0.005 497, –0.045 162	a_{35}	–0.021 734, 0.367 615	a_{77}	–0.000 005, –0.000 003

Note: The subscripts (1,2, …, 7) represent the corresponding variables (U_{10}, σ_0, $cvar$, λ_c/ β, sinθ, cos2φ, λ_{SAR}), e.g., a_{12} is the coefficient for the term of $U_{10}\times\sigma_0$.

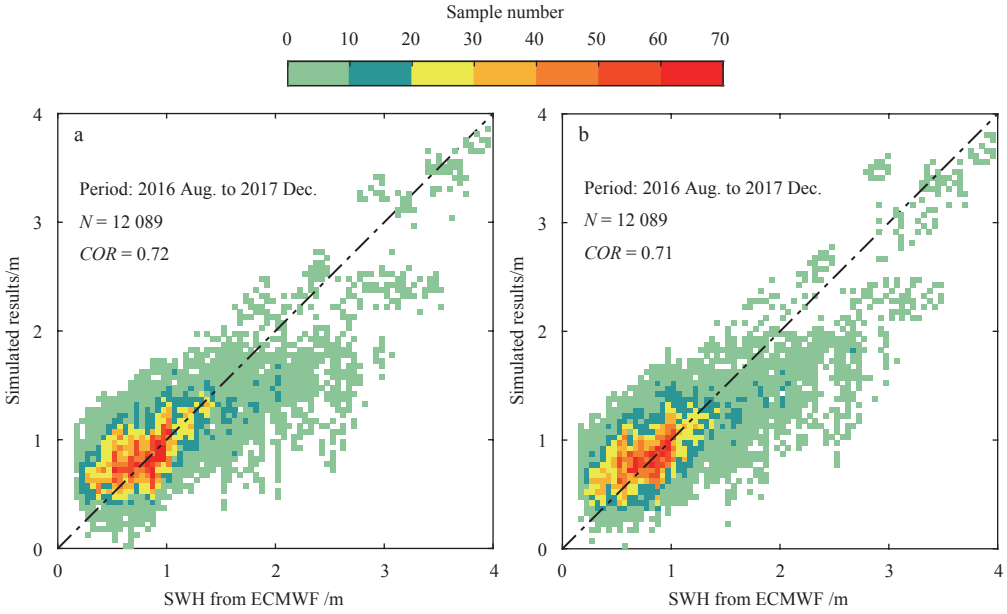

Fig. 4. Simulated results by using the empirical algorithm CSAR_WAVE2 vs. SWH from ECMWF reanalysis data for 0.1 m of SWH bins between 0 m and 3 m. a. VV-polarization and b. HH-polarization.

ments from NDBC buoys of NOAA shows an approximate 0.58 m RMSE of SWH for co-polarization using CSAR_WAVE (Shao et al., 2017b). This analysis shows that these algorithms all perform less well than the results achieved using CSAR_WAVE2, when non-linear higher-order corrections on sea state are included in CSAR_WAVE2. Therefore, it is recommended that CSAR_WAVE2 is applied operationally for wave retrieval from GF-3 SAR images in co-polarization. However, it is necessary to establish that there are no available data at high sea states in the fitting and validation procedure. CSAR_WAVE2 is expected to be further adopted for high sea states as the non-linearity is higher than at low and moderate sea states, especially in typhoons and hurricanes.

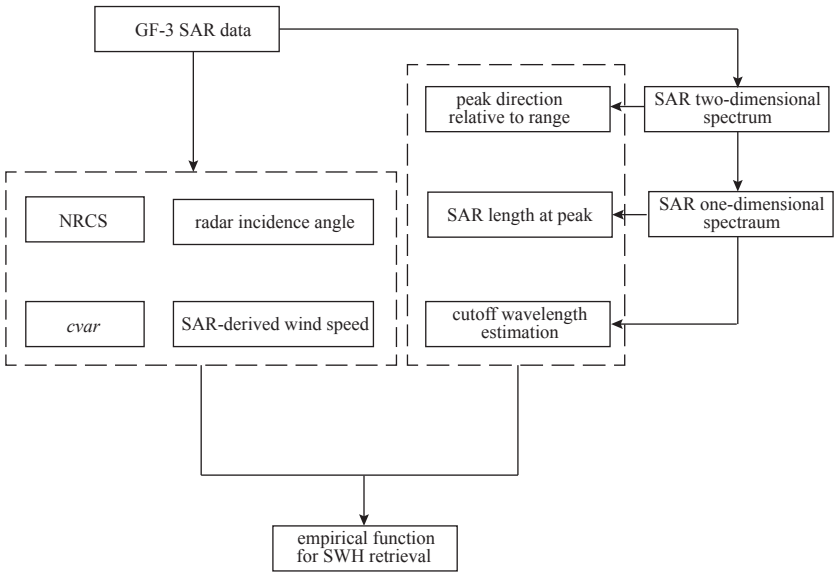

Fig. 5. The concise flowchart of SWH retrieval using CSAR_WAVE2, with reference to the application process of existing CWAVE and CSAR_WAVE models.

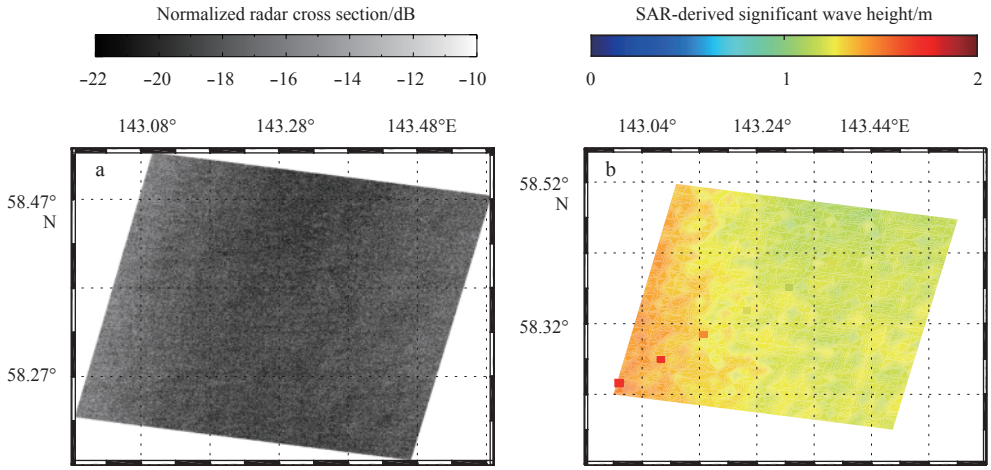

Fig. 6. The quick-look image of the VV-polarization GF-3 SAR image acquired at 20:49 UTC on 26 July 2017 (a) and the inverted wave map of this case using CSAR_WAVE2, in which the several small colored rectangles represent the SWH data measured from altimeter Jason-2 footprints (b).

5 Summary and conclusion

In the preliminary assessment (Shao et al., 2017b), the RMSE of SWH was around 0.58 m for GF-3 SAR when using the empirical wave retrieval algorithm CSAR_WAVE as validated against buoy measurements, which was tuned for S-1 SAR in VV-polarization. As for the operational application of GF-3 SAR, it is essential to reduce the retrieval error of the SWH for oceanic and coastal monitoring.

In this study, 1 523 GF-3 SAR images acquired in quad-polarization mode were collected during the period of August 2016 to December 2017. More than ten thousand sub-scenes from these images in the co-polarization channel were collocated with SWH from ECMWF reanalysis data at a 0.125° grid with SWH up to 4 m. Through the dataset, an improved wave retrieval algorithm for GF-3 SAR, denoted as CSAR_WAVE2, was developed. Seven variables, which are explicitly related to sea state and can be directly obtained from a SAR image, were selected for the CSAR_WAVE2 model. CSAR_WAVE2 is more than an updated version of CSAR_WAVE, as the formulation of function has been rigorously redesigned and non-linear higher-order corrections on sea state have been implemented. The COR is 0.72 and 0.71 for VV- and HH-polarization respectively, when the simulated SWH using CSAR_WAVE2 is compared with ECMWF reanalysis SWH data, indicating that CSAR_WAVE2 can be applied for wave retrieval from GF-3 SAR image in co-polarization.

An additional 92 GF-3 SAR images were collected, which cover the footprint of the altimeter Jason-2 mission. Validation shows that the RMSE of SWH is 0.51 m and 0.52 m for GF-3 SAR in VV- and HH-polarization respectively. We also compared the retrieval results with SWH of Jason-2 using three existing empirical algorithms (Wang et al., 2012; Ren et al., 2015; Grieco et al., 2016), showing a 0.60–0.70 m RMSE of SWH. As a result, it is concluded that the accuracy of retrieved SWH from co-polarization GF-3 SAR has been significantly improved using CSAR_WAVE2 at low to moderate sea states.

The applicability of CSAR_WAVE2 will be further investigated

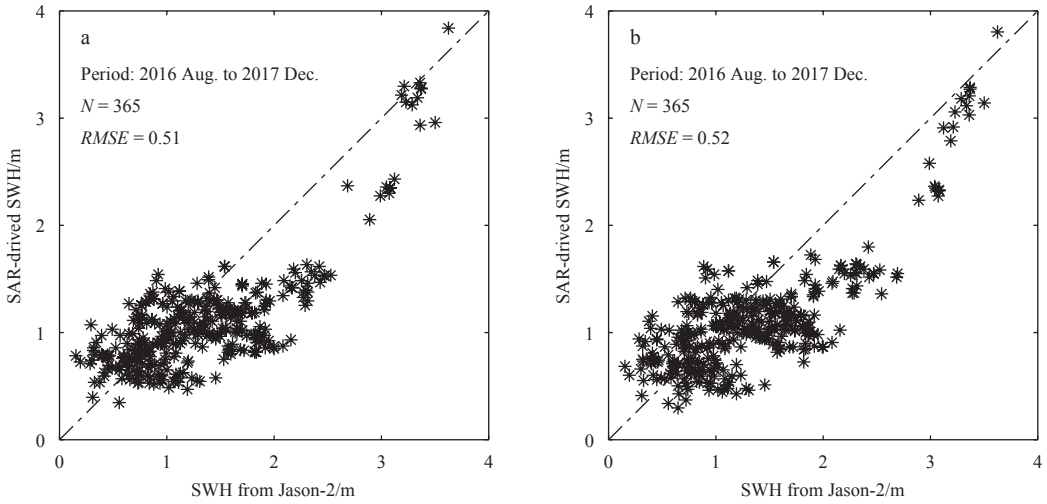

Fig. 7. SWH from Jason-2 vs. SAR-derived SWH from 92 GF-3 SAR images using CSAR_WAVE2. a. VV-polarization and b. HH-polarization.

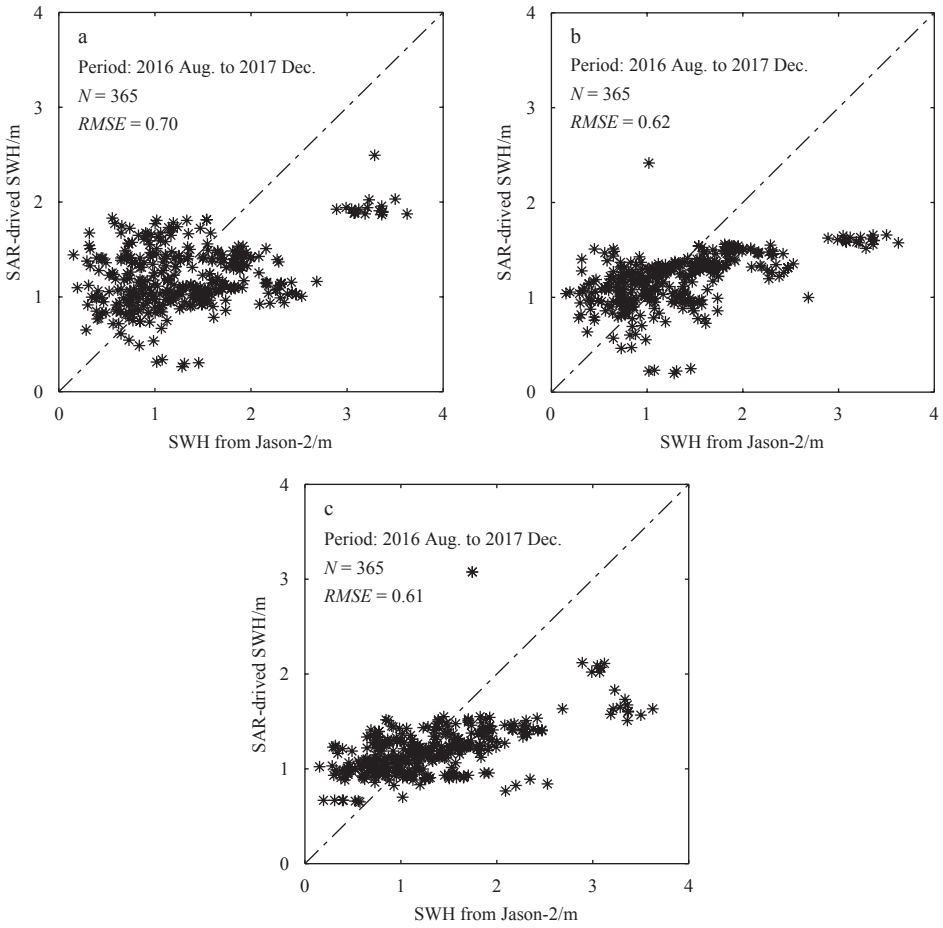

Fig. 8. SWH from Jason-2 vs. SAR-derived SWH from 92 VV-polarization GF-3 SAR images using three empirical algorithms, e.g., the results using the algorithm proposed by Wang et al. (2012) (a), the results using the algorithm proposed by Ren et al. (2015) (b), the results using the algorithm proposed by Grieco et al. (2016) (c).

for various GF-3 SAR data, e.g., Spotlight Mode (SL), Standard Stripmap (SS), Wide Scan (WSC), Global Observing Mode (GLO) and Wave Mode (WAV). Recently, GF-3 SAR has captured several typhoons by the National Ocean Satellite Application Center (NSOAS) around China's seas. Therefore, the applicability of CSAR_WAVE2 will be further investigated and can be adopted for high sea states in the near future.

Acknowledgements

Gaofen-3 synthetic aperture radar (SAR) images are collected through an authorized account issued by the National Ocean Satellite Application Center (NSOAS) under the contract of Specific Project of Chinese High Resolution Earth Observation System (No. 41-Y20A14-9001-15/16) via http://dds.nsoas.org.cn. The authers greatly appreciate the European Centre for Medium-Range Weather Forecasts (ECMWF) for providing reanalysis wind and wave data at a 0.125 grid, which were openly downloaded via http://www.ecmwf.int. Operational Geophysical Data Record (OGDR) wave data from Jason-2 mission were accessed via https://data.nodc.noaa.gov. The authers thank Cui Limin (NSOAS) and Li Huan (National Marine Data and Information Service) for the helpful discussions.

References

Abdalla S, Janssen P A E M, Bidlot J R. 2010. Jason-2 OGDR wind and wave products: monitoring, validation and assimilation. Marine Geodesy, 33(S1): 239–255

Alpers W, Brümmer B. 1994. Atmospheric boundary layer rolls observed by the synthetic aperture radar aboard the ERS-1 satellite. Journal of Geophysical Research, 99(C6): 12613–12621

Alpers W R, Ross D B, Rufenach C L. 1981. On the detectability of ocean surface waves by real and synthetic aperture radar. Journal of Geophysical Research: Oceans, 86(C7): 6481–6498

Alpers W R, Bruening C. 1986. On the relative importance of motion-related contributions to the Sar imaging mechanism of ocean surface waves. IEEE Transactions on Geoscience and Remote Sensing, GE-24(6): 873–885

Bruck M, Lehner S. 2015. TerraSAR-X/TanDEM-X sea state measurements using the XWAVE algorithm. International Journal of Remote Sensing, 36(15): 3890–3912

Chapron B, Johnsen H, Garello R. 2001. Wave and wind retrieval from SAR images of the ocean. Annales Des Télécommunications, 56(11–12): 682–699

Feindt F, Schröter J, Alpers W. 1986. Measurement of the ocean wave-radar modulation transfer function at 35 GHz from a sea-based platform in the North Sea. Journal of Geophysical Research: Oceans, 91(C8): 9701–9708

Grieco G, Lin W, Migliaccio M, et al. 2016. Dependency of the sentinel-1 azimuth wavelength Cut-off on significant wave height and wind speed. International Journal of Remote Sensing, 37(21): 5086–5104

Hasselmann K, Hasselmann S. 1991. On the nonlinear mapping of an ocean wave spectrum into a synthetic aperture radar image spectrum and its inversion. Journal of Geophysical Research: Oceans, 96(C6): 10713–10729

Hasselmann S, Hasselmann K. 1985. Computations and parametrizations of the nonlinear energy transfer in a gravity wave spectrum: Part I. a new method for efficient computations of the exact nonlinear transfer integral. Journal of Physical Oceanography, 15: 1369–1377

Hasselmann S, Bruning C, Hasselmann K. 1996. An improved algorithm for the retrieval of ocean wave spectra from synthetic aperture radar image spectra. Journal of Geophysical Research: Oceans, 101(C7): 16615–16629

Hersbach H, Stoffelen A, De Haan S. 2007. An improved C-band scatterometer ocean geophysical model function: CMOD5. Journal of Geophysical Research: Oceans, 112(C3): C03006

Hwang P A, Fois F. 2015. Surface roughness and breaking wave properties retrieved from polarimetric microwave radar backscattering. Journal of Geophysical Research: Oceans, 120(5): 3640–3657

Li Xiaofeng, Pichel W, He Mingxia, et al. 2002. Observation of hurricane-generated ocean swell refraction at the gulf stream north wall with the RADARSAT-1 synthetic aperture radar. IEEE Transactions on Geoscience and Remote Sensing, 40(10): 2131–2142

Li Xiaoming, Koenig T, Schulz-Stellenfleth J, et al. 2010. Validation and intercomparison of ocean wave spectra inversion schemes using ASAR wave mode data. International Journal of Remote Sensing, 31(17): 4969–4993

Li Xiaoming, Lehner S, Bruns T. 2011. Ocean wave integral parameter measurements using envisat ASAR wave mode data. IEEE Transactions on Geoscience and Remote Sensing, 49(1): 155–174

Li Xiaofeng. 2015. The first sentinel-1 SAR image of a typhoon. Acta Oceanologica Sinica, 34(1): 1–2

Lin Bo, Shao Weizeng, Li Xiaofeng, et al. 2017. Development and validation of an ocean wave retrieval algorithm for VV-polarization sentinel-1 SAR Data. Acta Oceanologica Sinica, 36(7): 95–101

Lyzenga D R. 1986. Numerical simulation of synthetic aperture radar image spectra for ocean waves. IEEE Transactions on Geoscience and Remote Sensing, GE-24(6): 863–872

Marghany M, Ibrahim Z, Van Genderen J. 2002. Azimuth cut-off model for significant wave height investigation along coastal water of Kuala Terengganu, Malaysia. International Journal of Applied Earth Observation and Geoinformation, 4(2): 147–160

Mastenbroek C, De Valk C F. 2000. A semiparametric algorithm to retrieve ocean wave spectra from synthetic aperture radar. Journal of Geophysical Research: Oceans, 105(C2): 3497–3516

Pleskachevsky A L, Rosenthal W, Lehner S. 2016. Meteo-marine parameters for highly variable environment in coastal regions from satellite radar images. ISPRS Journal of Photogrammetry and Remote Sensing, 119(2): 464–484

Ren Lin, Yang Jingsong, Zheng Gang, et al. 2015. Significant wave height estimation using azimuth Cutoff of C-band RADARSAT-2 single-polarization SAR images. Acta Oceanologica Sinica, 34(12): 93–101

Ren Lin, Yang Jingsong, Mouche A, et al. 2017. Preliminary analysis of Chinese GF-3 SAR Quad-polarization measurements to extract winds in each polarization. Remote Sensing, 9(12): 1215

Romeiser R, Graber H C, Caruso M J, et al. 2015. A new approach to ocean wave parameter estimates from C-band ScanSAR images. IEEE Transactions on Geoscience and Remote Sensing, 53(3): 1320–1345

Schulz-Stellenfleth J, Lehner S, Hoja D. 2005. A parametric scheme for the retrieval of two-dimensional ocean wave spectra from synthetic aperture radar look cross spectra. Journal of Geophysical Research: Oceans, 101(C5): C05004

Schulz-Stellenfleth J, König T, Lehner S. 2007. An empirical approach for the retrieval of integral ocean wave parameters from synthetic aperture radar data. Journal of Geophysical Research: Oceans, 112(C3): C03019

Shao Weizeng, Li Xiaofeng, Hwang P, et al. 2017a. Bridging the gap between cyclone wind and wave by C-band SAR measurements. Journal of Geophysical Research: Oceans, 122(8): 6714–6724

Shao Weizeng, Li Xiaofeng, Sun Jian. 2015. Ocean wave parameters retrieval from TerraSAR-X images validated against buoy measurements and model results. Remote Sensing, 7(10): 12815–12828

Shao Weizeng, Sheng Yexin, Sun Jian. 2017b. Preliminary assessment of wind and wave retrieval from Chinese Gaofen-3 SAR imagery. Sensors, 17(8): 1705

Shao Weizeng, Sun Jian, Guan Changlong, et al. 2014. A method for sea surface wind field retrieval from SAR image mode data. Journal of Ocean University of China, 13(2): 198–204

Shao Weizeng, Wang Jing, Li Xiaofeng, et al. 2017c. An empirical algorithm for wave retrieval from Co-polarization X-Band SAR imagery. Remote Sensing, 9(7): 711

Shao Weizeng, Yuan Xinzhe, Sheng Yexin, et al. 2018. Development of wind speed retrieval from cross-polarization Chinese Gaofen-3 synthetic aperture radar in typhoons. Sensors, 18(2): 412

Shao Weizeng, Zhang Zheng, Li Xiaofeng, et al. 2016. Ocean wave parameters retrieval from sentinel-1 SAR imagery. Remote Sensing, 8(9): 707

Stoffelen A, Anderson D. 1997. Scatterometer data interpretation: es-

timation and validation of the transfer function CMOD4. Journal of Geophysical Research: Oceans, 102(C3): 5767–5780

Stopa J E, Ardhuin F, Chapron B, et al. 2016. Estimating wave orbital velocity through the azimuth cutoff from space-borne satellites. Journal of Geophysical Research: Oceans, 120(11): 7616–7634

Stopa J E, Mouche A. 2017. Significant wave heights from sentinel-1 SAR: validation and applications. Journal of Geophysical Research: Oceans, 122(3): 1827–1848

Sun Jian, Guan Changlong. 2006. Parameterized first-guess spectrum method for retrieving directional spectrum of swell-dominated waves and huge waves from SAR images. Chinese Journal of Oceanology and Limnology, 24(1): 12–20

Sun Jian, Kawamura H. 2009. Retrieval of surface wave parameters from SAR images and their validation in the coastal seas around Japan. Journal of Oceanography, 65(4): 567

Wang He, Yang Jingsong, Mouche A, et al. 2017. GF-3 SAR ocean wind retrieval: the first view and preliminary assessment. Remote Sensing, 9(7): 694

Wang He, Zhu Jianhua, Yang Jingsong, et al. 2012. A semiempirical algorithm for SAR wave height retrieval and its validation using envisat ASAR wave mode data. Acta Oceanologica Sinica, 31(3): 59–66

Yang Jingsong, Wang Juan, Ren Lin. 2017. The first quantitative remote sensing of ocean internal waves by Chinese GF-3 SAR satellite. Acta Oceanologica Sinica, 36(1): 118

Zhang Biao, Perrie W, He Yijun. 2011. Wind speed retrieval from RADARSAT-2 quad-polarization images using a new polarization ratio model. Journal of Geophysical Research: Oceans, 116(C8): C08008